



**Superconducting phase transition in planar fermionic models with Dirac cone tilting**Y. M. P. Gomes <sup>1,\*</sup> and Rudnei O. Ramos <sup>1,2,†</sup><sup>1</sup>*Departamento de Física Teórica, Universidade do Estado do Rio de Janeiro, 20550-013 Rio de Janeiro, RJ, Brazil*<sup>2</sup>*Physics Department, McGill University, Montreal, Quebec H3A 2T8, Canada* (Received 21 April 2022; revised 27 February 2023; accepted 28 February 2023; published 8 March 2023)

The chiral and superconducting gaps are studied in the context of a planar fermion model with four-fermion interactions. The effect of the tilt of the Dirac cone on both gaps is shown and discussed. Our results point to two different behaviors exhibited by planar fermionic systems. We show that there is a threshold value  $\tilde{t}^*$  for the effective tilt parameter such that when  $|\tilde{t}| < \tilde{t}^*$ , the superconducting phase persists for negative values of the superconducting coupling constant. For positive values of the superconducting coupling constant, the induction of a superconducting gap by a chemical potential exists, which is similar to the one seen in graphenelike systems. For  $|\tilde{t}| > \tilde{t}^*$  and a negative superconducting coupling constant, the superconducting phase can be present, but it is restricted to a smaller area in the phase portrait. Our analysis also shows that when  $|\tilde{t}| > \tilde{t}^*$  and for positive values for the superconducting coupling constant, the induction of a superconducting gap in the presence of a chemical potential is ruled out. In this case, the increase of the chemical potential works in favor of the manifestation of a metallic phase.

DOI: [10.1103/PhysRevB.107.125120](https://doi.org/10.1103/PhysRevB.107.125120)**I. INTRODUCTION**

The possibility of the superconducting phase in the Weyl fermion system is one of the popular topics in condensed-matter physics. The discovery of a tilted Weyl dispersion in realistic materials, for example, type-II Weyl semimetals, has accelerated the related research on this topic. The detailed verification of the phase diagram for these types of systems is of relevance for researchers in the field. Here we approach this important problem from the point of view of quantum field theory techniques. Since the seminal work of Gross and Neveu [1], where the authors use quantum field theory (QFT) tools to describe two-dimensional massless fermions with quartic interactions, much attention was expended to apply QFT techniques in low-dimensional systems and with special attention to condensed-matter problems. One of the most interesting examples of the applications of QFT in condensate matter is the study of graphene [2]. In this almost planar system, the electrons obey linearly dispersing relations and the fermionic excitations are well described by a relativistic Dirac equation in (2+1) dimensions.

The Lorentz symmetry is respected by the electrons in graphene due to its relativistic characteristics, but this feature is an exception compared to the majority of materials in condensed matter. Some of the condensed-matter systems, where the dispersion in the proximity of band touching points can be generically linear and resemble the Weyl equation, do not respect Lorentz symmetry [3–6]. Even though there are quasiparticles in the aforementioned systems that behave like Weyl fermions [7], these systems are described by Weyl-like

Hamiltonians and, thus, these quasiparticles are by construction massless and more stable against gap formation in comparison to Dirac ones [8].

Our proposal in this paper is to study how the properties associated with Weyl fermions influence the formations of chiral and superconducting gaps in planar systems. Superconductivity was studied in three-dimensional Weyl semimetals of both types I and II with a particular effect of the tilting of the Dirac cone [9]. From the experimental side, despite the challenges, there have been studies in heterostructures consisting of thin films of half-metal and spin-singlet superconductor [10]. The theoretical study of superconducting instabilities in Dirac and Luttinger fermions has also been recently analyzed [11]. Here we will extend the usual Weyl Hamiltonian used in the description of Weyl semimetals (WSMs) [12,13] by introducing two forms of four-fermion interactions that will allow for a chiral phase and a superconducting phase. We also analyze the properties of this system under the effects of a finite chemical potential, which in practice models the doping process. This will allow us to study the allowed phase transitions in a (2 + 1)-dimensional Gross-Neveu (GN)-type model, which describes the competition between the chiral symmetry breaking and superconductivity. These two phenomena will dispute the true ground state of the system through the intensity of the coupling constants and as a function of the chemical potential. Let us also recall that chiral symmetry and its breaking can be seen as a way to describe the metal-insulator phase transition in these planar systems. Thus, the study of chiral symmetry breaking in planar systems by GN-like four-fermion interactions has become a useful tool for qualitative analysis of the two-dimensional system and has already been used successfully in many different contexts [14–32].

In this paper, we also want to address the question of the production of a superconducting phase in the model and

\*yurimullergomes@gmail.com

†rudnei@uerj.br

how the tilting of the Dirac cone affects it. The phenomenon of electron pairing in the vast majority of superconductors follows the Bardeen-Cooper-Schrieffer (BCS) theory of superconductivity. The BCS theory describes the condensation of electrons into pairs with antiparallel spins in a singlet state with an  $s$ -wave symmetry. The  $s$ -wave channel will be the superconducting channel that will be addressed in this paper. Several works have already indicated that superconductivity appears in planar systems, such as twisted bilayer graphene [33], normal trilayer graphene [34], and twisted trilayer graphene as well [35,36]. However, here we address the effects caused by the tilt of the Dirac cone on the combined chiral and superconducting phases and how it might influence, in particular, the superconducting gap.

The tilting, the coupling constants for the chiral and pairing interactions in the superconducting channel, and the chemical potential provide four independent parameters. From the coupling constants, we can present a phase diagram in the case where the tilt factor and the chemical potential take values that are of practical interest. In particular, we find that the existence of the superconducting phase strongly depends on whether the tilt factor is larger or smaller than a threshold value  $\tilde{t}^*$ , which we explicitly estimate both analytically and numerically, besides depending as well on the sign of the pairing interaction in the superconducting channel.

The remainder of this paper is organized as follows. In Sec. II, we briefly discuss the main properties of two-dimensional Dirac and Weyl semimetal systems. In Sec. III, we present the extension of the model that describes the four-fermion interactions for the excitonic and superconducting channels. The effective thermodynamic potential for the system is derived through the mean-field and one-loop semiclassical approximation level. The effects of the anisotropy, tilting of the Dirac cone, and chemical potential are taking into account in this derivation. In Sec. IV, we show and discuss the effect of the chemical potential  $\mu$  on the effective thermodynamic potential and we present the chiral and superconductivity gap equations of the system. In Sec. V, we discuss the phase transition of the system as a function of the chemical potential. In Sec. VI, our conclusions and remarks are presented, along with the discussion of the possible implications of our results to some current experimental planar materials of interest. Two Appendices are also included where some technical details are presented. Throughout this paper, we will be considering the natural units where  $\hbar = k_B = c = 1$ .

## II. TWO-DIMENSIONAL WEYL SEMIMETALS

In this section, we present the main details of the representation of the low-energy electronic excitations in the two-dimensional Weyl semimetals. Within the tight-binding approximation calculated for the honeycomblike lattices, the low-energy dynamics of the two-dimensional system of Weyl fermions can be described by the Hamiltonian [12,13]

$$H_I(\mathbf{p}) = v_F[\mathbf{t} \cdot \mathbf{p}]\tau^0 + (\xi_x p_x)\tau^x + (\xi_y p_y)\tau^y, \quad (2.1)$$

where  $v_F$  is the Fermi velocity,  $\mathbf{t}$  is called the tilt vector that describes the Dirac cone tilt,  $\xi = (\xi_x, \xi_y)$  is the vector

that describes the anisotropy of the material,  $\tau^0 = \mathbb{1}$  is the  $2 \times 2$  identity matrix, and  $\tau^{x,y}$  are the Pauli matrices. In the limit  $\mathbf{t} \rightarrow 0$  and  $\xi_x = \xi_y = 1$ , we recover the Hamiltonian of the isotropic graphene. The tilt vector  $\mathbf{t}$  is related to the separation between the Dirac cones in the Weyl semimetal. A consequence of the non-null tilt term in Eq. (2.1) is that the Dirac points, denoted by  $D$  and  $D'$ , no longer coincide with the Brillouin corners  $K$  and  $K'$  (see, e.g., Ref. [12]). In particular, type-I Weyl semimetals are characterized by  $|\mathbf{t}| < 1$ , while type-II ones are characterized by  $|\mathbf{t}| > 1$ . From the Hamiltonian given by Eq. (2.1), one finds that the spectrum is given by

$$E_\lambda(\mathbf{p}) = v_F[\mathbf{t} \cdot \mathbf{p} + \lambda\sqrt{(\xi_x p_x)^2 + (\xi_y p_y)^2}], \quad (2.2)$$

where  $\lambda = \pm 1$  represent the conduction and valence bands, respectively. Note that to be able to associate  $\lambda = +1$  with a positive and  $\lambda = -1$  with a negative energy state, it is required that [12,13]

$$\sqrt{\left(\frac{t_x}{\xi_x}\right)^2 + \left(\frac{t_y}{\xi_y}\right)^2} = |\tilde{\mathbf{t}}| < 1, \quad (2.3)$$

where  $|\tilde{\mathbf{t}}|$  is called the *effective tilt parameter*.

The Hamiltonian given by Eq. (2.1) commutes with the chirality operator defined as

$$C = \frac{(\xi_x p_x)\tau_x + (\xi_y p_y)\tau_y}{\sqrt{(\xi_x p_x)^2 + (\xi_y p_y)^2}}, \quad (2.4)$$

with the eigenvalues given by  $\alpha = \pm 1$ . Taking into account all the degeneracies of the system, the free Weyl fermion can be described with a four-component spinor, and a Dirac-like Lagrangian density can be written as follows (see, e.g., Ref. [37]):

$$\mathcal{L} = \sum_{k=1}^N i\bar{\psi}_k M^{\mu\nu} \gamma_\mu \partial_\nu \psi_k, \quad (2.5)$$

where  $\psi$  is a four-component Dirac fermion. The  $\gamma$  matrices are written as

$$\gamma^\mu = \tau^\mu \otimes \begin{pmatrix} 1 & 0 \\ 0 & -1 \end{pmatrix}, \quad (2.6)$$

with  $\mu = 0, 1, 2$ ,  $\tau^\mu = (\tau_z, i\tau_x, i\tau_y)$ ,  $\bar{\psi} = \psi^\dagger \gamma^0$ , and  $\tau_z$  is the third Pauli matrix. The  $\gamma$  matrices obey the identity  $\gamma^\mu \gamma^\nu = \eta^{\mu\nu} + i\epsilon^{\mu\nu\lambda} \gamma_3 \gamma_\lambda$ , where  $\gamma_3 = \begin{pmatrix} 1 & 0 \\ 0 & -1 \end{pmatrix}$  and  $\eta^{\mu\nu} = \text{diag}(+, -, -)$ . Thus, it is straightforward to prove that the  $\gamma$  matrices obey the algebra  $\{\gamma^\mu, \gamma^\nu\} = 2\eta^{\mu\nu}$ . The matrix  $M$  in Eq. (2.5) is explicitly given by

$$M = \begin{pmatrix} 1 & -v_F t_x & -v_F t_y \\ 0 & -v_F \xi_x & 0 \\ 0 & 0 & -v_F \xi_y \end{pmatrix}. \quad (2.7)$$

We can see  $M$  as representing an analog of an effective metric. One also notices that  $M^{\mu\nu}$  contains the parameters that explicitly break the Lorentz symmetry, which is a consequence of the tilting of the Dirac cone. It is easy to show that the Lagrangian density given by Eq. (2.5) has a discrete chiral

symmetry given by  $\psi \rightarrow \gamma_5 \psi$  and  $\bar{\psi} \rightarrow -\bar{\psi} \gamma_5$ , with

$$i\gamma_5 = \begin{pmatrix} 0 & \mathbb{1} \\ -\mathbb{1} & 0 \end{pmatrix}. \quad (2.8)$$

Throughout the next sections, one follows Ref. [37] and chooses the mass term that breaks the chiral symmetry as  $\bar{\psi} \psi$ .

### III. CHIRAL AND DIFERMION INTERACTIONS

To write an effective Lagrangian density that can describe the (2+1)-dimensional Weyl semimetal with both chiral symmetry breaking (excitonic pairing) and superconductivity (Cooper pairing), two forms of four-fermion interactions can be introduced [20]. One of them is a four-fermion interaction for the scalar fermion-antifermion and the other one is for the scalar difermion channel. The complete model can then be written as

$$\begin{aligned} \mathcal{L} = & \sum_{k=1}^N \bar{\psi}_k (iM^{\mu\nu} \gamma_\mu \partial_\nu + \gamma^0 \mu) \psi_k + \frac{G_1 v_F}{2N} \left( \sum_{k=1}^N \bar{\psi}_k \psi_k \right)^2 \\ & + \frac{G_2 v_F}{2N} \sum_{k=1}^N (\psi_k^T C \psi_k) \sum_{j=1}^N (\bar{\psi}_j C \bar{\psi}_j^T), \end{aligned} \quad (3.1)$$

where  $C = i\gamma^2$  is the charge conjugation matrix and  $G_1$  and  $G_2$  are the coupling constants for the chiral and difermion channels. The coupling constants  $G_1$  and  $G_2$  are negative for an attractive interaction, while they are positive for a repulsive interaction. The attractive/repulsive nature of the couplings will be decisive for the phase transition patterns analyzed in the subsequent sections. The effective action of the model can be expressed as

$$\begin{aligned} \exp(iS_{\text{eff}}) = & \int D\bar{\psi} D\psi D\Delta D\Delta^* D\sigma \\ & \times \exp \left\{ \int d^3x \left[ \frac{N}{2G_1 v_F} \sigma^2 + \frac{N}{2G_2 v_F} \Delta^* \Delta \right. \right. \\ & + \sum_{k=1}^N \bar{\psi}_k (iM^{\mu\nu} \gamma_\mu \partial_\nu + \gamma^0 \mu + \sigma) \psi_k \\ & \left. \left. + \frac{\Delta^*}{2} \psi_k^T C \psi_k + \frac{\Delta}{2} \bar{\psi}_k C \bar{\psi}_k^T \right] \right\}, \end{aligned} \quad (3.2)$$

where  $\sigma = \frac{G_1 v_F}{N} \sum_{j=1}^N \bar{\psi}_j \psi_j$ ,  $\Delta = \frac{G_2 v_F}{N} \sum_{j=1}^N \psi_j^T C \psi_j$ , and  $\Delta^* = \frac{G_2 v_F}{N} \sum_{j=1}^N \bar{\psi}_j C \bar{\psi}_j^T$ . We can explicitly integrate over the fermion field (for the technical details, see Appendix A) and the effective action can be rewritten as  $S_{\text{eff}}(\sigma, \Delta, \Delta^*) = N \int d^3x \Omega(\sigma, \Delta, \Delta^*)$ , where  $\Omega$  is the effective thermodynamics potential,

$$\begin{aligned} \Omega(\sigma, \Delta, \Delta^*) = & \frac{1}{2G_1 v_F} \sigma^2 + \frac{1}{2G_2 v_F} \Delta^* \Delta \\ & + \sum_{i=1}^2 \int \frac{d^3p}{(2\pi)^3} \ln \lambda_i(p), \end{aligned} \quad (3.3)$$

with  $\lambda_i$  denoting the eigenvalues of  $B = CDC^{-1}D^T - |\Delta|^2$ ,

with  $D = M^{\mu\nu} \gamma_\mu \partial_\nu + \gamma^0 \mu - \sigma$ , which are given by

$$\begin{aligned} \lambda_{1,2} = & \sigma^2 + [p_0 - v_F(\mathbf{t} \cdot \mathbf{p})]^2 - v_F^2 \tilde{\mathbf{p}}^2 - \mu^2 - |\Delta|^2 \\ & \pm 2\sqrt{\sigma^2 \{ [p_0 - v_F(\mathbf{t} \cdot \mathbf{p})]^2 - v_F^2 \tilde{\mathbf{p}}^2 \} + v_F^2 \mu^2 \tilde{\mathbf{p}}^2}, \end{aligned} \quad (3.4)$$

with  $\tilde{\mathbf{p}} = (\xi_x p_x, \xi_y p_y)$ . Using the identity

$$\int_{-\infty}^{\infty} dp_0 \ln(p_0 - A) = i\pi |A|, \quad (3.5)$$

we find that

$$\sum_{i=1}^2 \int \frac{d^3p}{(2\pi)^3} \ln \lambda_i(p) = - \int \frac{d^2p}{(2\pi)^2} (|\Sigma^+| + |\Sigma^-|), \quad (3.6)$$

where

$$\Sigma^\pm = v_F(\mathbf{t} \cdot \mathbf{p}) + \sqrt{\tilde{E}^2 + \mu^2 + |\Delta|^2 \pm 2\sqrt{\sigma^2 |\Delta|^2 + \mu^2 \tilde{E}^2}}, \quad (3.7)$$

and  $\tilde{E}^2 = v_F^2 \tilde{\mathbf{p}}^2 + \sigma^2$ . Finally, for constant configurations  $\sigma_0 = \langle \sigma \rangle$  and  $\Delta_0 = \langle \Delta \rangle = \langle \Delta^* \rangle$ , we find

$$\begin{aligned} \Omega(\sigma_0, \Delta_0, \mu) = & \frac{1}{2G_1 v_F} \sigma_0^2 + \frac{1}{2G_2 v_F} \Delta_0^2 \\ & - \int \frac{d^2p}{(2\pi)^2} (|\Sigma_0^+| + |\Sigma_0^-|), \end{aligned} \quad (3.8)$$

where  $\Sigma_0^\pm = \Sigma^\pm(\sigma = \sigma_0, \Delta = \Delta_0)$ . Note that the momentum integral in Eq. (3.8) is divergent in the ultraviolet limit and, thus, the effective potential given by Eq. (3.8) needs to be renormalized. The renormalization of Eq. (3.8) is described below.

#### A. Renormalization

Taking  $\mu = 0$  in Eq. (3.8), we will have that  $\Sigma_0^\pm = \mathbf{t} \cdot \mathbf{p} + \sqrt{\tilde{\mathbf{p}}^2 + (\sigma_0 \pm \Delta_0)^2}$  and, therefore,

$$\begin{aligned} \Omega(\sigma_0, \Delta_0) = & \frac{1}{2G_1 v_F} \sigma_0^2 + \frac{1}{2G_2 v_F} \Delta_0^2 \\ & - \int \frac{d^2p}{(2\pi)^2} |v_F(\mathbf{t} \cdot \mathbf{p}) + \sqrt{v_F^2 \tilde{\mathbf{p}}^2 + (\sigma_0 + \Delta_0)^2}| \\ & - \int \frac{d^2p}{(2\pi)^2} |v_F(\mathbf{t} \cdot \mathbf{p}) + \sqrt{v_F^2 \tilde{\mathbf{p}}^2 + (\sigma_0 - \Delta_0)^2}|. \end{aligned} \quad (3.9)$$

The linear term  $\mathbf{t} \cdot \mathbf{p}$  in Eq. (3.9) vanishes in the integration over the angular variable,<sup>1</sup> but the integral in Eq. (3.9) is still divergent. Thus, applying the rescaling  $\xi_{x,y} p_{x,y} \rightarrow p_{x,y}$  and integrating with the introduction of a momentum cutoff  $\Lambda$ ,

<sup>1</sup>We use the identity  $\int_0^{2\pi} d\theta |a \cos \theta + b| = 2\pi b \Theta(b-a)$ , where  $\Theta(x)$  is the Heaviside function, for  $a > 0$  and  $b > 0$ .

one defines the renormalization conditions,

$$\begin{aligned} \frac{1}{g_1(m)} &= v_F \frac{d^2 \Omega(\sigma_0, \Delta_0)}{d\sigma_0^2} \Big|_{\sigma_0=m, \Delta_0=0} \\ &= \frac{1}{G_1} + \frac{2m}{\pi v_F \xi_x \xi_y} - \frac{\Lambda}{\pi v_F \xi_x \xi_y} \end{aligned} \quad (3.10)$$

and

$$\begin{aligned} \frac{1}{g_2(m')} &= v_F \frac{d^2 \Omega(\sigma_0, \Delta_0)}{d\Delta_0^2} \Big|_{\sigma_0=0, \Delta_0=m'} \\ &= \frac{1}{G_2} + \frac{2m'}{\pi v_F \xi_x \xi_y} - \frac{\Lambda}{\pi v_F \xi_x \xi_y}, \end{aligned} \quad (3.11)$$

where  $m$  and  $m'$  are regularization scales. Going further, defining the renormalized couplings  $g_1$  and  $g_2$  as

$$\frac{1}{g_1} = \frac{1}{g_1(m)} - \frac{2m}{\pi v_F \xi_x \xi_y} \quad (3.12)$$

and

$$\frac{1}{g_2} = \frac{1}{g_2(m')} - \frac{2m'}{\pi v_F \xi_x \xi_y}, \quad (3.13)$$

the renormalized effective thermodynamic potential finally can be expressed as

$$\begin{aligned} \Omega^{\text{ren}}(\sigma_0, \Delta_0) &= \frac{1}{2g_1 v_F} \sigma_0^2 + \frac{1}{2g_2 v_F} \Delta_0^2 \\ &+ \frac{(\sigma_0 + \Delta_0)^3}{6\pi v_F^2 \xi_x \xi_y} + \frac{|\sigma_0 - \Delta_0|^3}{6\pi v_F^2 \xi_x \xi_y}. \end{aligned} \quad (3.14)$$

### B. Phase diagram of the system at $\mu = 0$

Let us first specialize in the analysis of the effective thermodynamic potential and its properties in the case of a null chemical potential. In this perspective, we analyze the two sectors, the chiral and the superconductor ones, individually. This will allow us to extract the main characteristics of the model. After this analysis, we can then compare the results and show where each phase will be mandatory in the system.

The minima of Eq. (3.14) are given in terms of the gaps  $\bar{\sigma}_c$  and  $\bar{\Delta}_c$ , which are defined as  $\bar{\sigma}_c = \pi v_F \xi_x \xi_y / |g_1|$  and  $\bar{\Delta}_c = \pi v_F \xi_x \xi_y / |g_2|$ . By analyzing the thermodynamic potential given by Eq. (3.14), in the absence of tilting, it can be established that the system can be characterized by three phases, according to the values of  $\sigma$ ,  $\Delta$ , and the coupling constants. We follow the same classification used in Ref. [21] which studied the nontilted system. *Phase I*: this is the symmetric phase, where both vacuum expectations values for the chiral and superconducting phases are zero,  $\sigma_0 = \Delta_0 = 0$ , and which can take place when  $g_1 > 0$  and  $g_2 > 0$ . *Phase II*: in this phase,  $\sigma_0 = \bar{\sigma}_c \neq 0$  and  $\Delta_0 = 0$  and it can happen when  $g_1 < 0$ . *Phase III*: in this phase,  $\sigma_0 = 0$  and  $\Delta_0 = \bar{\Delta}_c \neq 0$  and it can happen when  $g_2 < 0$ . When  $g_1$  and  $g_2$  are simultaneously negative, the system is characterized as phase II if  $|g_1| > |g_2|$  and as phase III for  $|g_1| < |g_2|$ . In the next two sections, we will analyze how the effects of both tilting and chemical potential affect these different phases allowed by the model.

## IV. TILTING EFFECTS ON THE SUPERCONDUCTING GAP

Let us now turn on the effects of the tilting of the Dirac cone on the different three phases allowed by the model and described at the end of Sec. III. It is useful to first focus on the pure chiral phase (when  $\Delta_0 = 0$ ), where we here briefly reproduce some of the results obtained in Ref. [37]. After that, we will analyze the case of the superconducting gap in detail.

### A. The pure chiral phase ( $\Delta_0 = 0$ )

By considering the pure chiral phase, i.e., by considering  $\Delta_0 = 0$ , one notices that

$$(\Sigma_0^\pm)_{\Delta_0=0} = \mathcal{E}_\sigma^\pm = v_F(\mathbf{t} \cdot \mathbf{p}) + |\tilde{E}_0 \pm \mu|, \quad (4.1)$$

where  $\tilde{E}_0 = \sqrt{v_F^2 \tilde{\mathbf{p}}^2 + \sigma_0^2}$ . Assuming  $\mu > 0$ , one finds in this case that the effective thermodynamic potential (3.14) becomes

$$\begin{aligned} \Omega^{\text{ren}}(\sigma_0, 0, \mu) &= \frac{\sigma_0^2}{2g_1 v_F} + \frac{\sigma_0^3}{3\pi v_F^2 \xi_x \xi_y} \\ &- \int \frac{d^2 p}{(2\pi)^2} (|\mathcal{E}_\sigma^+| + |\mathcal{E}_\sigma^-| - 2E_\sigma) \\ &= \frac{\sigma_0^2}{2g_1 v_F} + \frac{\sigma_0^3}{3\pi v_F^2 \xi_x \xi_y} - \int \frac{d^2 p}{(2\pi)^2} (\mu - \tilde{E}_\sigma + |\mu - \tilde{E}_\sigma|) \\ &= \frac{\sigma_0^2}{2g_1 v_F} + \frac{\sigma_0^3}{3\pi v_F^2 \xi_x \xi_y} - 2 \int \frac{d^2 p}{(2\pi)^2} (\mu - \tilde{E}_\sigma) \Theta(\mu - \tilde{E}_\sigma), \end{aligned} \quad (4.2)$$

with  $\tilde{E}_\sigma = v_F(\mathbf{t} \cdot \mathbf{p}) + \sqrt{v_F^2 \tilde{\mathbf{p}}^2 + \sigma_0^2}$  and we have used the identity  $x + |x| = 2x\Theta(x)$ . From Eq. (4.2), one can derive the gap equation,

$$1 + \frac{\text{sign}(g_1)\sigma_0}{\bar{\sigma}_c} + 2g_1 \int \frac{d^2 p}{(2\pi)^2} \frac{\Theta(\mu - \tilde{E}_\sigma)}{\sqrt{v_F^2 \tilde{\mathbf{p}}^2 + \sigma_0^2}} = 0. \quad (4.3)$$

It follows from Eq. (4.3) that for  $g_1 > 0$ , the chiral symmetry is maintained for any  $\mu > 0$ . We can also see that the effect of the effective tilt parameter  $|\tilde{\mathbf{t}}|$  in Eq. (4.3) is to enhance the effect of the chemical potential and, hence, to lower the point of chiral symmetry restoration. In particular, for  $g_1 < 0$ , the chiral symmetry breaks for  $\mu < \mu_c$  and is restored for  $\mu > \mu_c$ , where the critical chemical potential  $\mu_c$  is found to be given by [37]

$$\mu_c = \sqrt{1 - |\tilde{\mathbf{t}}|^2 \bar{\sigma}_c}. \quad (4.4)$$

Therefore, we can say that the presence of the nonvanishing tilt parameter tends to facilitate the chiral symmetry restoration. One also finds from Eq. (4.3) that the chiral order parameter, which is the solution of (4.3), jumps discontinuously from  $\sigma_0 = \bar{\sigma}_c$  to  $\sigma_0 = 0$  as we change the chemical potential from  $\mu < \mu_c$  to  $\mu > \mu_c$ . This is a first-order transition that exists for both the nontilted case  $|\tilde{\mathbf{t}}| = 0$  and the tilted case  $|\tilde{\mathbf{t}}| \neq 0$ .

The charge density  $n$  is defined as

$$n = -N \frac{\partial \Omega^{\text{ren}}(\sigma_0, 0, \mu)}{\partial \mu} \Big|_{\sigma_0=(\sigma_0)}. \quad (4.5)$$

The exact expression for  $n$  can be readily calculated from  $\Omega^{\text{ren}}(\sigma_0, 0, \mu)$  and it reads

$$n(g_1 > 0) = \frac{N\mu^2}{2\pi v_F^2 \xi_x \xi_y (1 - |\tilde{\mathbf{t}}|^2)^{3/2}}, \quad (4.6)$$

when  $g_1 > 0$ , and

$$n(g_1 < 0) = \frac{N(\mu^2 - \mu_c^2)}{2\pi v_F^2 \xi_x \xi_y (1 - |\tilde{\mathbf{t}}|^2)^{3/2}} \Theta(\mu^2 - \mu_c^2), \quad (4.7)$$

when  $g_1 < 0$ .

In the next section, one turns to the analysis of the superconducting phase.

### B. The pure superconducting phase ( $\sigma_0 = 0$ )

In the case of a pure superconducting phase, i.e., considering now  $\sigma_0 = 0$ , and using the identity

$$(\Sigma_0^\pm)|_{\sigma_0=0} = \mathcal{E}_\Delta^\pm = v_F(\mathbf{t} \cdot \mathbf{p}) + \sqrt{(v_F|\tilde{\mathbf{p}}| \pm \mu)^2 + \Delta_0^2}, \quad (4.8)$$

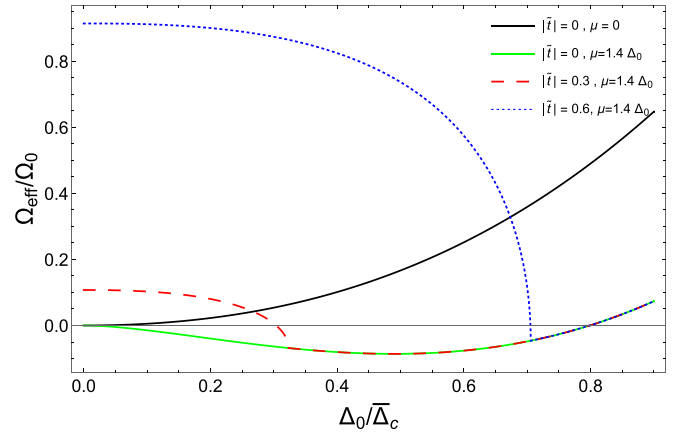
the effective thermodynamic potential (3.14) can be written as

$$\begin{aligned} \Omega^{\text{ren}}(0, \Delta_0, \mu) &= \frac{\Delta_0^2}{2g_2 v_F} + \frac{\Delta_0^3}{3\pi v_F^2 \xi_x \xi_y} \\ &- \int \frac{d^2 p}{(2\pi)^2} \{ |\mathcal{E}_\Delta^+| + |\mathcal{E}_\Delta^-| \\ &- 2[v_F(\mathbf{t} \cdot \mathbf{p}) + \sqrt{v_F^2 |\tilde{\mathbf{p}}|^2 + \Delta_0^2}] \}. \end{aligned} \quad (4.9)$$

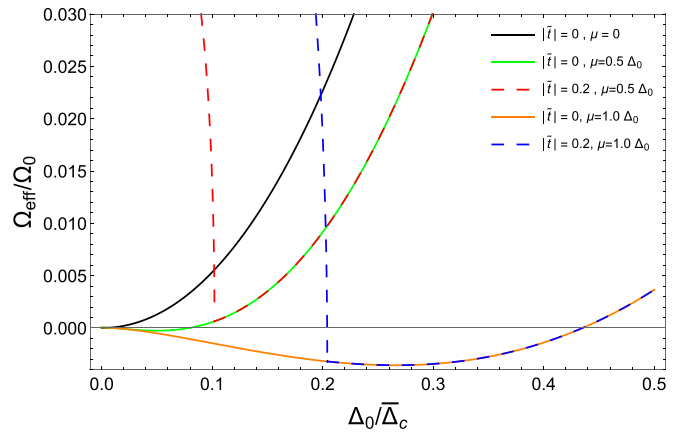
Performing the momentum integrals in Eq. (4.9), one finds

$$\begin{aligned} \Omega^{\text{ren}}(0, \Delta_0, \mu) &= \frac{\Delta_0^2}{2g_2 v_F} + \frac{(\mu^2 + \Delta_0^2)^{3/2}}{3\pi v_F^2 \xi_x \xi_y} \\ &- \frac{\mu^2 \sqrt{\mu^2 + \Delta_0^2}}{2\pi v_F^2 \xi_x \xi_y} - \frac{\mu \Delta_0^2}{2\pi v_F^2 \xi_x \xi_y} \ln \left( \frac{\mu + \sqrt{\mu^2 + \Delta_0^2}}{\Delta_0} \right) \\ &+ \frac{1}{2\pi \xi_x \xi_y v_F^2} I(\Delta_0, \mu), \end{aligned} \quad (4.10)$$

where the function  $I(\Delta_0, \mu)$  is derived explicitly in Appendix B and given by Eq. (B8). The effective thermodynamic potential given by Eq. (4.10) is shown in Fig. 1(a) for  $g_2 < 0$ , while for  $g_2 > 0$  it is shown in Fig. 1(b) for  $g_2 > 0$ , where we have considered some representative values of the effective tilt parameter and for the chemical potential. The emergence of a superconducting gap  $\Delta \neq 0$  due to the combined effect of the tilt and chemical potential is noted. Let us analyze in more details the contribution of the tilt parameter for the superconducting gap. New features generated by the tilt of the Dirac cone will influence the superconducting gap for both the  $g_2 > 0$  and  $g_2 < 0$  scenarios and are explained below.



(a)  $g_2 < 0$



(b)  $g_2 > 0$

FIG. 1. Effective thermodynamic potential for (a)  $g_2 < 0$  and (b)  $g_2 > 0$ , in units of  $\Omega_0 = N\bar{\Delta}_c^3/(\pi v_F^2 \xi_x \xi_y)$  as a function of  $\Delta/\bar{\Delta}_c$ .

From the effective thermodynamic potential, one derives the gap equation,

$$\begin{aligned} \text{sign}(g_2) + \sqrt{x^2 + y^2} - y \ln \left( \frac{y + \sqrt{x^2 + y^2}}{x} \right) \\ + \frac{1}{2x} \frac{\partial I(x, y)}{\partial x} = 0, \end{aligned} \quad (4.11)$$

where  $x = \Delta_0/\bar{\Delta}_c$ ,  $y = \mu/\bar{\Delta}_c$ . The superconducting gap that is induced by the chemical potential and the tilt parameter is shown in Figs. 2(a) and 2(b), for the cases of  $g_2 < 0$  and for  $g_2 > 0$ , respectively.

In Fig. 2, the numerical results for the superconducting gap are shown as a function of the chemical potential and some representative values for the effective tilt parameter  $|\tilde{\mathbf{t}}|$ .

In the case  $g_2 < 0$ , which is shown in Fig. 2(a), one can see that the tilt increases  $\Delta_c$  for a given  $\mu > \mu_c^*$ . In the particular value  $\mu_c^* = \mu_c^*(|\tilde{\mathbf{t}}|)$  is where the tilt parameter starts to contribute to the superconducting gap. The behavior of  $\mu_c^*$  as a function of  $|\tilde{\mathbf{t}}|$  is shown in Fig. 3. We find that there is a threshold value for the effective tilt parameter  $\tilde{t}^*$ , such that when  $|\tilde{\mathbf{t}}| < \tilde{t}^*$ , the superconducting gap is given by  $\Delta_0 = \Delta_{t=0}$  for any  $\mu$ . However, for values of  $|\tilde{\mathbf{t}}| > \tilde{t}^*$  and when  $\mu > \mu_c^*$ , the superconducting gap is given by  $\Delta_0 = \Delta_t$ .



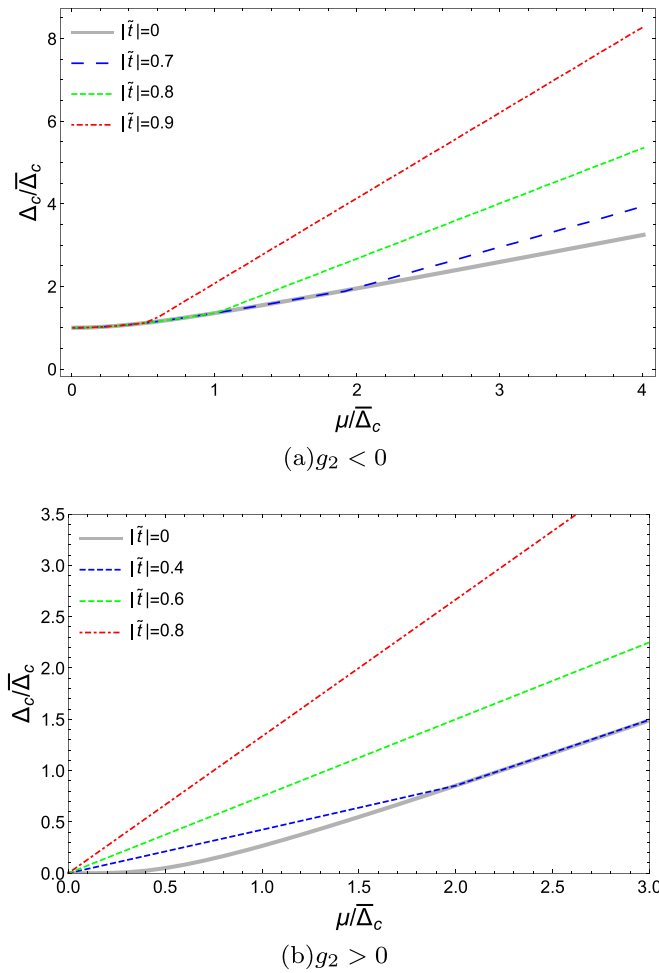


FIG. 2. Superconducting gap for (a)  $g_2 < 0$  and (b)  $g_2 > 0$  induced by the chemical potential and the tilt parameter in units of  $\Delta_c$  for some representative values of  $|\tilde{t}|$ .

On the other hand, in the case of  $\mu < \mu_{<}^*$ , the superconducting gap is given instead again by  $\Delta_0 = \Delta_{t=0}$ . Let us obtain an explicit estimation for this particular value for the effective tilt parameter  $\tilde{t}^*$ . For  $\mu > \mu_{<}^*$ , the superconducting gap takes

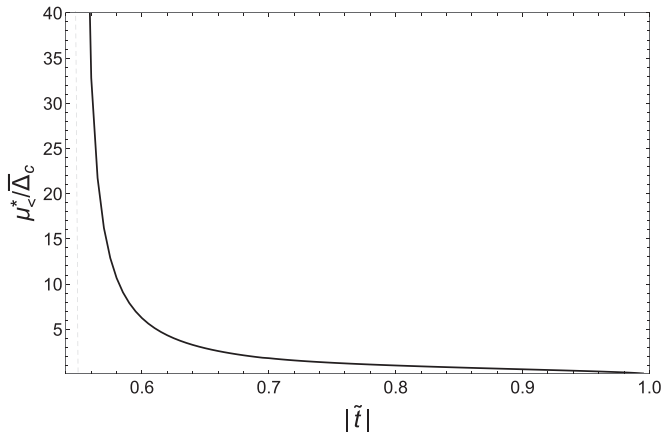


FIG. 3. The normalized chemical potential  $\mu_{<}^*$  as a function of  $|\tilde{t}|$ . The thin vertical dashed line represents the threshold value  $|\tilde{t}| = \tilde{t}^*$ .

the exact form  $\Delta_c(\mu > \mu_{<}^*) = \Delta_t$ , where

$$\Delta_t = \frac{|\tilde{t}|\mu}{\sqrt{1 - |\tilde{t}|^2}}. \quad (4.12)$$

Moreover, in order to extract the asymptotic behavior of the superconducting gap shown in Fig. 2, one first notes that in the gap equation for the nontilted case ( $\tilde{t} = 0$ ), the last term in Eq. (4.11) vanishes. Hence, for  $\tilde{t} = 0$ ,

$$\text{sign}(g_2) + \sqrt{x^2 + y^2} - y \ln \left( \frac{y + \sqrt{x^2 + y^2}}{x} \right) = 0.$$

Now, it is reasonable to assume that in the large- $y$  limit, the normalized gap solution  $x$  becomes a linear function of the normalized chemical potential  $y$ , i.e.,  $x = \lambda y + c$ , with  $c$  a constant. Hence, considering the asymptotic limit  $y, x \ll c$  and multiplying Eq. (4.13) by  $1/y$ , one obtains that  $\lambda$  satisfies

$$\sqrt{\lambda^2 + 1} - \ln \left( \frac{\sqrt{\lambda^2 + 1} + 1}{\lambda} \right) \approx 0. \quad (4.13)$$

The above equation has one positive solution given by  $\lambda \simeq 0.66$ . The threshold value  $\tilde{t}^*$  for which the effective tilt parameter begins to drive the superconducting gap is determined when the superconducting gap, given by Eq. (4.12), becomes parallel to the asymptotic linear behavior of the tiltless gap equation, i.e., we must have  $\Delta_t = \lambda\mu$ . This leads to the relation

$$\frac{|\tilde{t}|}{\sqrt{1 - |\tilde{t}|^2}} = \lambda. \quad (4.14)$$

The solution of the above equation gives us the result  $\tilde{t}^* \simeq 0.55$  when using the solution for  $\lambda$  obtained from Eq. (4.14). This result agrees quite well with the numerical results expected from Figs. 2 and 3.

When  $g_2 < 0$ , for any value of the tilt parameter  $|\tilde{t}| < \tilde{t}^*$ , the effect of the tilt parameter in the superconducting gap vanishes for any  $\mu$ , and the superconducting gap of the system obeys the solid gray curve shown in Fig. 2(a). We can also analyze the situation for the case of  $g_2 > 0$ . Analyzing now the case for  $g_2 > 0$ , we are able to uncover another structure for the superconducting gap. As can be seen in Fig. 2(b), in this case we have two different situations. When  $|\tilde{t}| < \tilde{t}^*$ , the tilt parameter only contributes for the chemical potential up to the values  $\mu_{>}^*$ ,  $\mu < \mu_{>}^*$ , e.g., as in the case seen by the blue curve in Fig. 2(b). This particular value  $\mu_{>}^* = \mu_{>}^*(|\tilde{t}|)$  sets a lower limit where the tilt parameter stops contributing to the superconducting gap. The behavior of  $\mu_{>}^*$  is shown in Fig. 4. When  $|\tilde{t}| > \tilde{t}^*$ , the superconducting gap will be exactly  $\Delta_c(|\tilde{t}| > \tilde{t}^*) = \Delta_t$ . As seen in Fig. 4, we now have that when  $g_2 > 0$ , for values of  $\mu > \mu_{>}^*$  the superconducting gap is given by  $\Delta_0 = \Delta_{t=0}$ , and for  $\mu < \mu_{>}^*$  the superconducting gap is given by  $\Delta_0 = \Delta_t$ . For  $|\tilde{t}| > \tilde{t}^*$ , the superconducting gap is given by  $\Delta_0 = \Delta_t$  for any  $\mu$ .

Finally, we can explicitly compute the charge density,

$$n = -N \left. \frac{\partial \Omega^{\text{ren}}(\Omega, \Delta_0, \mu)}{\partial \mu} \right|_{\Delta_0 = (\Delta_0)}, \quad (4.15)$$

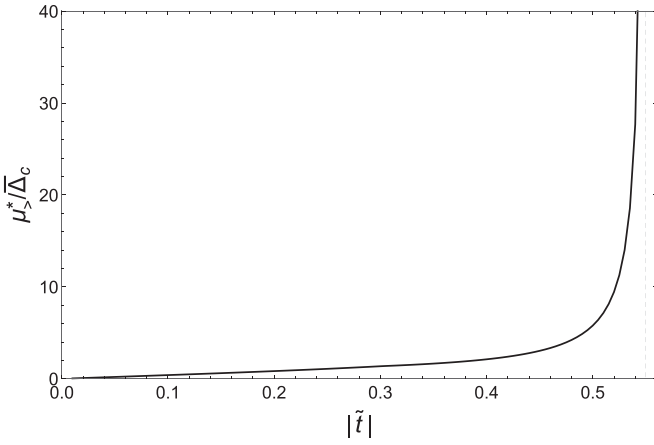


FIG. 4. Plot of the normalized chemical potential  $\mu^*$ . The thin vertical dashed line represents the threshold value  $|\tilde{t}| = \tilde{t}^*$ .

which can be expressed through an exact expression and given by

$$n = \frac{N}{4\pi v_F^2 \xi_x \xi_y} \left[ \mu \sqrt{\mu^2 + \Delta_0^2} + \Delta_0^2 \ln \left( \frac{\mu + \sqrt{\mu^2 + \Delta_0^2}}{\Delta_0} \right) \right] \Big|_{\Delta_0 = \langle \Delta_0 \rangle} + N \frac{\partial I(\Delta_0, \mu)}{\partial \mu} \Big|_{\Delta_0 = \langle \Delta_0 \rangle}, \quad (4.16)$$

where  $\langle \Delta_0 \rangle$  is the solution of Eq. (4.11), which can be found numerically for both the  $g_2 > 0$  and  $g_2 < 0$  cases. From the inequality  $\text{Re} \sqrt{|\tilde{t}|^2 \mu^2 - (1 - |\tilde{t}|^2) \Delta_0^2} \neq 0$ , one finds that the contribution for the charge density from the function  $I$  is non-null only for  $\langle \Delta_0 \rangle < \Delta_t$ . Thus, based on Fig. 2(a), this contribution is non-null only for  $\mu < \mu^*$ . In the case where  $g_2 > 0$ , on the other hand, from Fig. 2(b), the density will receive extra contributions only for  $\mu > \mu^*$ .

## V. PHASE STRUCTURE FOR $\mu \neq 0$

Previous works [20,20,23,24] have shown that it is sufficient to analyze the chiral-superconducting phase structure by comparing the vacuum properties in the  $\sigma_0 = 0$  and  $\Delta_0 = 0$  axes. Here we follow the same strategy. Through this analysis of the local minimum in each axis, we can compare them and find the global minimum which defines the real phase of the system. For instance, as shown in the previous section, for fixed  $g_1 < 0$ , there is a chemical potential for coexistence,  $\mu_c(g_2)$ . The value of  $\mu_c(g_2)$  defines the lower bound for the chemical potential such that for  $\mu > \mu_c(g_2)$ , the system is in the superconducting phase (phase III), for  $\mu < \mu_c(g_2)$  the system is in the chiral symmetry-breaking phase (phase II), and for  $\mu = \mu_c(g_2)$  both phases II and III coexist. This coexistence point  $\mu = \mu_c(g_2)$  defines a first-order transition between phases II and III. In the case of  $g_2 < 0$ , there is another particular value for the chemical potential,  $\mu^*$ , as discussed in the previous section, such that for  $\mu > \mu^*$ , the superconducting phase stops to drive the system in favor

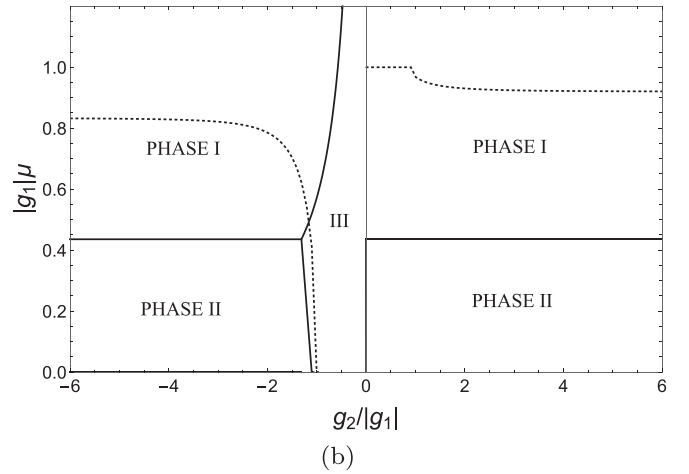
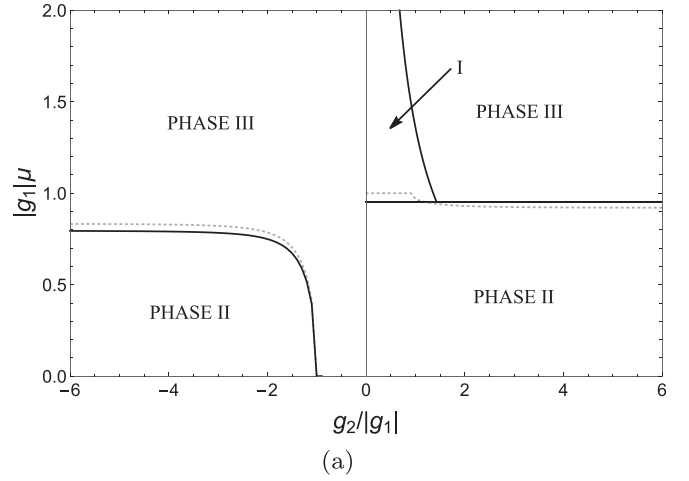


FIG. 5. Phase portrait for the normalized chemical potential ( $|g_1|\mu$ ) vs  $g_2/|g_1|$  for  $g_1 < 0$  and when (a)  $|\tilde{t}| = 0.3 < \tilde{t}^*$  and (b)  $|\tilde{t}| = 0.9 > \tilde{t}^*$ . The thin dashed lines represent the value for the chemical potential of coexistence in the nontilted case. Phases I, II, and III represent the metallic phase (with  $\sigma_0 = \Delta_0 = 0$ ), the insulating phase (with  $\sigma_0 \neq 0$  and  $\Delta_0 = 0$ ), and the superconducting phase (with  $\sigma_0 = 0$  and  $\Delta_0 \neq 0$ ), respectively.

of the chiral phase. The opposite happens when  $g_2 > 0$ , in which case there is now a value for the chemical potential,  $\mu = \mu^*$ , that becomes an upper bound and, for  $\mu < \mu^*$ , it is when the superconducting phase stops to drive the system in favor of the chiral phase. Finally, the chiral symmetry will be restored for  $\mu > \sqrt{1 - |\tilde{t}|^2} \bar{\sigma}_c$ . Let us now show the different phase portraits that will display the above structure relating the chemical potential with the superconducting coupling constant  $g_2$  of the system when assuming  $g_1 < 0$ , which is the relevant situation for nontrivial chiral and superconducting gaps.

For illustration, in Fig. 5(a), we show the phase portrait when  $|\tilde{t}| = 0.3 < \tilde{t}^*$  and in the region ranging from negative to positive values for  $g_2$ , while in Fig. 5(b), the phase portrait is shown for the case  $|\tilde{t}| = 0.9 > \tilde{t}^*$ . For reference, in both Figs. 5(a) and 5(b), the phase portrait in the nontilted case,  $|\tilde{t}| = 0$ , is shown by the light-gray dashed line, which matches the result previously obtained in Ref. [20]. Note that in the

nontilted case,  $|\tilde{\mathbf{t}}| = 0$ , the lines of coexistence separate phase II, which lies below the dashed line, from phase III, which lies above it. There is no phase I (where the chiral and superconducting phases are absent) in this case. Looking at the region where  $g_2 < 0$  in the case  $|\tilde{\mathbf{t}}| < \tilde{t}^*$  shown in Fig. 5(a), it is apparent that the presence of the effective tilt parameter  $|\tilde{\mathbf{t}}|$  does not qualitatively change the phase portrait with respect to that of the nontilted case. The structure of the phase transition can be summarized as a first-order phase transition between the insulating phase and the superconducting phase for a given  $\mu_c(g_2)$ , represented by the black line. In this case, the superconducting phase is present for  $\mu > \mu_c(g_2)$  in the same manner as in the nontilted situation. Looking now at the region where  $g_2 > 0$  for the case  $|\tilde{\mathbf{t}}| < \tilde{t}^*$ , also shown in Fig. 5(a), one can notice that the superconductivity induced by the chemical potential still exists, but in a smaller area when compared to the nontilted case (dashed line). We recall that from the results shown in the previous section, for  $\mu < \mu_>$  and when  $\mu > \sqrt{1 - |\tilde{\mathbf{t}}|^2} \bar{\sigma}_c$ , phase I takes place. Thus, in this case, one finds a point of coexistence,  $(\mu^t, g_2^t)$ , which separates phases I–III, which is given by

$$(\mu^t, g_2^t) \Big|_{g_2 > 0, |\tilde{\mathbf{t}}| < \tilde{t}^*} = \left( \frac{\sqrt{1 - |\tilde{\mathbf{t}}|^2}}{|g_1|}, \frac{\sqrt{1 - |\tilde{\mathbf{t}}|^2}}{\mu_>} \right). \quad (5.1)$$

The presence of the coexistence point as a consequence of the tilt of the Dirac cone is one of our main results, showing a quite different behavior when compared to the results in the nontilted case [20].

Going further, looking at the case for  $g_2 < 0$  and  $|\tilde{\mathbf{t}}| > \tilde{t}^*$ , which is shown in Fig. 5(b), one notices a much stronger change in the phase portrait as compared to the region with  $g_2 < 0$  shown in Fig. 5(a). The presence of the tilt effectively causes the superconducting gap to stop to drive the system for  $\mu > \mu_<$  and phase I now takes place for  $\mu > \sqrt{1 - |\tilde{\mathbf{t}}|^2} \bar{\sigma}_c$ . The phase portrait in this case displays a much restricted area for the superconducting phase. The superconducting phase occurs only for values of  $|g_2|/|g_1| \lesssim 1$ . In this case, one coexistence point also appears and it is found to be given by

$$(\mu^t, g_2^t) \Big|_{g_2 < 0, |\tilde{\mathbf{t}}| > \tilde{t}^*} = \left( \frac{\sqrt{1 - |\tilde{\mathbf{t}}|^2}}{|g_1|}, -\frac{\sqrt{1 - |\tilde{\mathbf{t}}|^2}}{\mu_<} \right). \quad (5.2)$$

Finally, looking at the region where  $g_2 > 0$  shown in Fig. 5(b), the induction of a superconducting phase due to the chemical potential is ruled out for any value of the chemical potential and the phase transition occurs between phases I and II. Through the increase of the chemical potential and in the presence of a tilt satisfying  $|\tilde{\mathbf{t}}| > \tilde{t}^*$ , both effects work in favor of the chiral symmetric phase. This can be seen by the enlarged region for phase I shown in Fig. 5(b) when compared to the nontilted case. This is our other main result that is extracted from the phase portrait. It shows once more the effect of the tilt on hindering the formation of gaps in the system and, in this case, the formation of an induced gap due to the presence of the chemical potential. The role of the threshold value for the effective tilt parameter  $\tilde{t}^*$  becomes quite evident when contrasting the two panels in Fig. 5.

## VI. CONCLUDING REMARKS

In this paper, we have investigated the phase diagram of the Weyl fermion system with four-fermion interactions that introduce the effects of both chiral and superconducting gaps. Furthermore, we have focused on the effect of the tilt factor of the Dirac cone. As one of our main results, it is the demonstration, both analytically and numerically, of the presence of a threshold value for the effective tilt parameter  $\tilde{t}^*$  beyond which the value of the tilting of the Dirac cone strongly affects the superconducting gap. More specifically, one explicitly finds that  $\tilde{t}^* \simeq 0.55$ . The stability of the superconducting phase is also found to be much different, whether the tilting factor is lower or higher than  $\tilde{t}^*$ . At this value for the effective tilt parameter, the system behaves completely differently under the formation of the chiral and superconducting gaps when compared to the nontilted case. In the case where  $|\tilde{\mathbf{t}}| < \tilde{t}^*$ , the superconducting phase persists for a negative superconducting coupling constant, which is responsible for the attractive interaction in the Cooper channel. A first-order phase transition occurs for a chemical potential for coexistence, as seen by the black curve in Fig. 5(a). This feature is similar to the results for graphene and other two-dimensional materials [20]. One also sees that for  $g_2 > 0$ , the induction of a superconducting gap due to the presence of a chemical potential exists. This induction, however, only happens for stronger values of the coupling constant  $g_2$  since the metallic phase appears for small values of the superconducting coupling constant. Due to the presence of a metallic phase, we were able to find the expression for the point of coexistence, which is given by Eq. (5.1).

While for values of  $|\tilde{\mathbf{t}}| < \tilde{t}^*$  the changes to the phase portrait seen in Fig. 5(a) are of a qualitative nature, when the effective tilt exceeds the threshold value, the changes now become quantitative. When  $|\tilde{\mathbf{t}}|$  exceeds the value  $\tilde{t}^*$ , the superconducting phase now becomes restricted to a smaller area in the phase portrait. Indeed, in this case, the superconducting phase occurs only for regions with small and negative superconducting coupling constant. Through a first-order phase transition, the metallic phase takes place for a sufficient large superconducting coupling constant and chemical potential. One also finds the analytic expression for the point of coexistence in this case, which is given by Eq. (5.2). Finally, one shows that our qualitative analysis points to the fact that for  $g_2 > 0$ , the superconducting gap induced by the chemical potential is ruled out and a first-order phase transition occurs between phases I and II at the chemical potential for coexistence, which is represented by the black curve in Fig. 5(b). The presence and role of the threshold value for the effective tilt parameter represent one of the main important results shown in this paper.

We can try to explore the consequences of the results we have obtained for some known planar systems which have been currently studied in laboratory experiments. For example, using the experimental data obtained from the two-dimensional (2D) organic conductor  $\alpha - (\text{BEDT-TTF})_2\text{I}_3$  [38,39], the estimated effective tilt parameter is found to be  $|\tilde{\mathbf{t}}| \simeq 0.76$  (see, e.g., Ref. [37]). This case occurs in the situation where  $|\tilde{\mathbf{t}}| > \tilde{t}^* \simeq 0.55$ , which we have discovered in this paper. From our results, this implies that the inducing of



a superconducting gap should be absent in this material. It would be interesting to probe this prediction using this type of material in the laboratory. By also accounting for the results obtained from the analysis of Ref. [37], we can also conclude that this same system should exhibit a metallic phase, which would become very strong under doping. On the other hand, we can also compare with the predictions that our results would imply for the case of quinoid-type graphene under uniaxial strain [12]. In this case, the estimated values for the effective tilt parameter are such that  $|\tilde{\mathbf{t}}| \lesssim 0.06$  for moderate deformations. From our results, we can conclude that for this material, the properties of the superconducting gap should be similar to the graphene case, which includes the induction of a superconducting gap by the chemical potential. To the authors' best knowledge, we are not aware of other materials where the value of the tilt parameter has been provided, at least as far as two-dimensional materials are concerned. We are hopeful that as new two-dimensional materials are experimentally probed and fabricated, new data from those experiments will help to shed light on the results we have presented here.

The study of possible two-dimensional fermionic systems where our results can be of interest can be exploited in several directions. First, since the evaluation of  $\tilde{r}^*$  is based on the large- $N$  limit of the effective thermodynamical potential, it is possible that this result receives quantum corrections beyond the large- $N$  approximation. This can be an interesting extension of the present work. Going further, the presence of an anomalous Hall effect [37,40,41] in the 2D Weyl semimetal indicates the possibility that the tilt of the Dirac cones could modify the superconducting gap under the presence of an external magnetic field. Moreover, since the tilt of the Dirac cone introduces a special direction in the system, the analysis of the  $p$ -wave superconducting gap properties in this context could bring new features. This can be another problem of interest that can be a target of further investigation. These problems are possible lines of study that our results motivate and we hope to address them in the future.

### ACKNOWLEDGMENTS

Y.M.P.G. is supported by a postdoctoral grant from Fundação Carlos Chagas Filho de Amparo à Pesquisa do Estado do Rio de Janeiro (FAPERJ). R.O.R. acknowledges financial support of the Coordenação de Aperfeiçoamento de Pessoal de Nível Superior (CAPES) - Finance Code 001 and by research grants from Conselho Nacional de Desenvolvimento Científico e Tecnológico (CNPq), Grant No. 307286/2021-5, and from Fundação Carlos Chagas Filho de Amparo à Pesquisa do Estado do Rio de Janeiro (FAPERJ), Grant No. E-26/201.150/2021.

### APPENDIX A: PERFORMING THE PATH INTEGRAL OVER THE FERMION IN EQ. (3.2)

Here we show some of the details of the path integral over the fermions in Eq. (3.2), which leads to the effective thermodynamic potential. Adopting the procedure described in Ref. [20], we assume two anticommuting four-component Dirac spinor fields  $q(x)$  and  $\bar{q}(x)$ . Then, Eq. (3.2) can be

rewritten as

$$I = \int DqD\bar{q} e^{i \int d^3x [\bar{q} \mathcal{O} q - \frac{\Delta}{2} q^T C q - \frac{\Delta^*}{2} \bar{q} C \bar{q}^T]}, \quad (\text{A1})$$

where  $\mathcal{O} = iM^{\mu\nu} \gamma_\mu \partial_\nu + \mu \gamma^0 - \sigma$  and  $C = i\gamma^2$  is the charge conjugation matrix. Using the Gaussian path integral identities

$$\int Dp e^{i \int d^3x [-\frac{1}{2} p^T A p + \eta^T p]} = (\det A)^{\frac{1}{2}} e^{-\frac{i}{2} \int d^3x \eta^T A^{-1} \eta} \quad (\text{A2})$$

and

$$\int D\bar{p} e^{i \int d^3x [-\frac{1}{2} \bar{p} A \bar{p}^T + \eta \bar{p}^T]} = (\det A)^{\frac{1}{2}} e^{-\frac{i}{2} \int d^3x \bar{\eta} A^{-1} \eta^T}, \quad (\text{A3})$$

and by also considering  $A = \Delta C$ ,  $\bar{q} \mathcal{O} = \eta^T$ ,  $\mathcal{O}^T \bar{q}^T = \eta$ , one finds, after integrating over  $q$  and  $\bar{q}$ , the result

$$\begin{aligned} I &= \int DqD\bar{q} e^{i \int d^3x [\bar{q} \mathcal{O} q - \frac{\Delta}{2} q^T C q - \frac{\Delta^*}{2} \bar{q} C \bar{q}^T]} \\ &= (\det \Delta C)^{\frac{1}{2}} \int D\bar{q} e^{\frac{i}{2} \int d^3x [\bar{q} (\Delta^* C + \mathcal{O} (\Delta C)^{-1} \mathcal{O}^T) \bar{q}^T]} \\ &= (\det \Delta C)^{\frac{1}{2}} \{\det [\Delta^* C + \mathcal{O} (\Delta C)^{-1} \mathcal{O}]\}^{\frac{1}{2}} \\ &= [\det (\Delta^2 + \mathcal{O} C^{-1} \mathcal{O}^T C)]^{\frac{1}{2}}, \end{aligned} \quad (\text{A4})$$

where we have assumed  $\Delta = \Delta^*$  in the last step [we are not interested in the phase of the superconducting order parameter, but solely on its absolute (modulus) value]. Using the relations  $C^{-1} \gamma_\mu^T C = -\gamma_\mu$  and  $\partial_\mu^T = -\partial_\mu$ , one finds that

$$I = [\det (-\Delta^2 + \mathcal{O}_+ \mathcal{O}_-)]^{1/2} = (\det B)^{\frac{1}{2}}, \quad (\text{A5})$$

with  $\mathcal{O}_\pm = iM^{\mu\nu} \gamma_\mu \partial_\nu \pm \mu \gamma^0 - \sigma$ . Finally, using the identity  $\det B = \exp(\text{Tr} \ln B)$ , one finds

$$\ln I = \frac{1}{2} \text{tr}(\ln B) = \int d^3x \sum_{i=1}^2 \int \frac{d^3p}{(2\pi)^3} \ln \lambda_i(p), \quad (\text{A6})$$

where

$$\begin{aligned} \lambda_{1,2} &= \sigma^2 + [p_0 - v_F(\mathbf{t} \cdot \mathbf{p})]^2 - v_F^2 \tilde{\mathbf{p}}^2 - \mu^2 - |\Delta|^2 \\ &\pm 2\sqrt{\sigma^2 \{ [p_0 - v_F(\mathbf{t} \cdot \mathbf{p})]^2 - v_F^2 \tilde{\mathbf{p}}^2 \} + v_F^2 \mu^2 \tilde{\mathbf{p}}^2} \end{aligned} \quad (\text{A7})$$

are the eigenvalues of  $B$ .

### APPENDIX B: THE EFFECTIVE THERMODYNAMIC POTENTIAL

In this section, one shows some of the details for the derivation of the effective thermodynamic potential. From Eq. (4.9), we obtain

$$\begin{aligned} \Omega^{\text{ren}}(0, \Delta_0, \mu) &= \frac{\Delta_0^2}{2g_2 v_F} + \frac{\Delta_0^3}{3\pi v_F^2 \xi_x \xi_y} \\ &- \int \frac{d^2p}{(2\pi)^2} \{ |\mathcal{E}_\Delta^+| + |\mathcal{E}_\Delta^-| \\ &- 2[v_F(\mathbf{t} \cdot \mathbf{p}) + \sqrt{v_F^2 |\tilde{\mathbf{p}}|^2 + \Delta_0^2}] \}, \end{aligned} \quad (\text{B1})$$

where  $\mathcal{E}_\Delta^\pm = v_F(\mathbf{t} \cdot \mathbf{p}) + \sqrt{(v_F|\tilde{\mathbf{p}}| \pm \mu)^2 + \Delta_0^2}$ . The effective thermodynamic potential depends on momentum integrals of the form

$$i_\pm = \int \frac{d^2p}{(2\pi)^2} \{ |\mathcal{E}_\Delta^\pm| - [v_F(\mathbf{t} \cdot \mathbf{p}) + \sqrt{v_F^2|\tilde{\mathbf{p}}|^2 + \Delta_0^2}] \}. \quad (\text{B2})$$

Then,  $\Omega^{\text{ren}}(0, \Delta_0, \mu)$  can be written as

$$\Omega^{\text{ren}}(0, \Delta_0, \mu) = \frac{\Delta_0^2}{2g_2v_F} + \frac{\Delta_0^3}{3\pi v_F^2 \xi_x \xi_y} - i_+ - i_-. \quad (\text{B3})$$

It can now be shown that for  $\mu > 0$ ,  $\mathcal{E}_\Delta^+ > 0$  for all  $p > 0$ . Hence, after some algebraic steps, one finds

$$i_+ = \frac{1}{2\pi v_F^2 \xi_x \xi_y} \int_0^\infty dpp [\sqrt{(p+\mu)^2 + \Delta_0^2} - \sqrt{p^2 + \Delta_0^2}]. \quad (\text{B4})$$

For  $\mathcal{E}_\Delta^-$ , one has that  $\mathcal{E}_\Delta^- > 0$  only for  $p < p_-$  and for  $p > p_+$ , where

$$p_\pm = \frac{1}{(1 - |\tilde{\mathbf{t}}|^2)} [\mu \pm \text{Re} \sqrt{|\tilde{\mathbf{t}}|^2 \mu^2 - (1 - |\tilde{\mathbf{t}}|^2) \Delta_0^2}], \quad (\text{B5})$$

where Re means the real part. From the above expressions, then, it follows that

$$\begin{aligned} & \int \frac{d^2p}{(2\pi)^2} |\mathcal{E}_\Delta^-| \\ &= \frac{1}{2\pi v_F^2 \xi_x \xi_y} \\ & \times \int_0^\infty dpp \int_0^{2\pi} \frac{d\theta}{(2\pi)} [|\tilde{\mathbf{t}}|p \cos \theta + \sqrt{(p-\mu)^2 + \Delta_0^2}] \\ &= \frac{1}{2\pi v_F^2 \xi_x \xi_y} \int_0^\infty dpp \sqrt{(p-\mu)^2 + \Delta_0^2} \\ & \Theta[\sqrt{(p-\mu)^2 + \Delta_0^2} - \tilde{\mathbf{t}}|p], \end{aligned} \quad (\text{B6})$$

where we have used the identity  $\int_0^{2\pi} \frac{d\theta}{2\pi} |a \cos \theta + b| = b\Theta(b-a)$  for  $a > 0$  and  $b > 0$  in the last step, and  $\Theta(x)$  is the Heaviside function. Finally, the inequality  $\sqrt{(p-\mu)^2 + \Delta_0^2} - \tilde{\mathbf{t}}|p > 0$  is respected when  $p < p_-$  and  $p > p_+$ . In particular, one notes that in the limit  $|\tilde{\mathbf{t}}| \rightarrow 0$ , one finds  $p_+ = p_- = \mu$ . Therefore, using the fact that  $\int_0^{p_-} + \int_{p_+}^\infty = \int_0^\infty - \int_{p_-}^{p_+}$ , it follows that

$$\begin{aligned} i_- &= \frac{1}{2\pi v_F^2 \xi_x \xi_y} \int_0^\infty dpp [\sqrt{(p-\mu)^2 + \Delta_0^2} - \sqrt{p^2 + \Delta_0^2}] \\ & - \frac{1}{2\pi v_F^2 \xi_x \xi_y} \int_{p_-}^{p_+} dpp \sqrt{(p-\mu)^2 + \Delta_0^2} \\ &= \frac{1}{2\pi v_F^2 \xi_x \xi_y} \left\{ \int_0^\infty dpp [\sqrt{(p-\mu)^2 + \Delta_0^2} - \sqrt{p^2 + \Delta_0^2}] \right. \\ & \left. - I(\Delta_0, \mu) \right\}, \end{aligned} \quad (\text{B7})$$

where

$$\begin{aligned} I(\Delta_0, \mu) &= \int_{p_-}^{p_+} dpp \sqrt{(p-\mu)^2 + \Delta_0^2} \\ &= (2\Delta_0^2 - \mu^2 + 2p_+^2 - \mu p_+) \sqrt{\Delta_0^2 + (p_+ - \mu)^2} \\ & + 3\Delta_0^2 \mu \tanh^{-1} \left[ \frac{p_+ - \mu}{\sqrt{\Delta_0^2 + (p_+ - \mu)^2}} \right] \\ & - (2\Delta_0^2 - \mu^2 + 2p_-^2 - \mu p_-) \sqrt{\Delta_0^2 + (p_- - \mu)^2} \\ & - 3\Delta_0^2 \mu \tanh^{-1} \left[ \frac{p_- - \mu}{\sqrt{\Delta_0^2 + (p_- - \mu)^2}} \right]. \end{aligned} \quad (\text{B8})$$

In normalized units  $x = \Delta_0/\bar{\Delta}_c$ ,  $y = \mu/\bar{\Delta}_c$ ,  $I(x, y)$  is given by

$$\begin{aligned} I(x, y) &= (2x^2 - y^2 + 2z_+^2 - yz_+) \sqrt{x^2 + (z_+ - y)^2} \\ & + 3x^2 y \tanh^{-1} \left[ \frac{z_+ - y}{\sqrt{x^2 + (z_+ - y)^2}} \right] \\ & - (2x^2 - y^2 + 2z_-^2 - yz_-) \sqrt{x^2 + (z_- - y)^2} \\ & - 3x^2 y \tanh^{-1} \left[ \frac{z_- - y}{\sqrt{x^2 + (z_- - y)^2}} \right], \end{aligned} \quad (\text{B9})$$

with  $z_\pm$  defined as

$$z_\pm = \frac{1}{(1 - |\tilde{\mathbf{t}}|^2)} [y \pm \text{Re} \sqrt{|\tilde{\mathbf{t}}|^2 y^2 - (1 - |\tilde{\mathbf{t}}|^2) x^2}]. \quad (\text{B10})$$

Finally, after integration over the momentum  $p$ , one can write the renormalized effective thermodynamic potential for the superconducting phase (when  $\sigma_0 = 0$ ) as

$$\begin{aligned} \Omega^{\text{ren}}(0, \Delta_0, \mu) &= \frac{\Delta_0^2}{2g_2v_F} + \frac{(\mu^2 + \Delta_0^2)^{3/2}}{3\pi v_F^2 \xi_x \xi_y} - \frac{\mu^2 \sqrt{\mu^2 + \Delta_0^2}}{2\pi v_F^2 \xi_x \xi_y} \\ & - \frac{\mu \Delta_0^2}{2\pi v_F^2 \xi_x \xi_y} \ln \left( \frac{\mu + \sqrt{\mu^2 + \Delta_0^2}}{\Delta_0} \right) \\ & + \frac{1}{2\pi \xi_x \xi_y v_F^2} I(\Delta_0, \mu). \end{aligned} \quad (\text{B11})$$

- [1] D. J. Gross and A. Neveu, Dynamical symmetry breaking in asymptotically free field theories, *Phys. Rev. D* **10**, 3235 (1974).
- [2] K. S. Novoselov, A. K. Geim, S. V. Morozov, D. Jiang, M. I. Katsnelson, I. V. Grigorieva, S. V. Dubonos, and A. A. Firsov, Two-dimensional gas of massless Dirac fermions in graphene, *Nature (London)* **438**, 197 (2005).
- [3] D. Grassano, O. Pulci, E. Cannuccia, and F. Bechstedt, Influence of anisotropy, tilt and pairing of Weyl nodes: The Weyl semimetals TaAs, TaP, NbAs and NbP, *Eur. Phys. J. B* **93**, 157 (2020).
- [4] L. Zhang, Y. Jiang, D. Smirnov, and Z. Jiang, Landau quantization in tilted Weyl semimetals with broken symmetry, *J. Appl. Phys.* **129**, 105107 (2021).
- [5] V. A. Kostelecký, R. Lehnert, N. McGinnis, M. Schreck, and B. Seradjeh, Lorentz violation in Dirac and Weyl semimetals, *Phys. Rev. Res.* **4**, 023106 (2022).
- [6] Y. Tamashevich, L. D. M. Villari, and M. Ornigotti, Nonlinear optical response of type-II Weyl fermions in two dimensions, *Phys. Rev. B* **105**, 195102 (2022).
- [7] H. Weyl, Electron and gravitation 1, *Z. Phys.* **56**, 330 (1929).
- [8] S. Y. Xu, I. Belopolski, N. Alidoust, M. Neupane, G. Bian, C. Zhang, R. Sankar, G. Chang, Z. Yuan, C. C. Lee *et al.* Discovery of a Weyl fermion semimetal and topological Fermi arcs, *Science* **349**, 613 (2015).
- [9] B. Rosenstein, B. Y. Shapiro, D. Li, and I. Shapiro, Magnetic properties of type-I and type-II Weyl semimetals in the superconducting state, *Phys. Rev. B* **97**, 144510 (2018).
- [10] L. Hao and C. S. Ting, Searching for two-dimensional Weyl superconductors in heterostructures, *Phys. Rev. B* **95**, 064513 (2017).
- [11] A. L. Szabó and B. Roy, Extended Hubbard model in undoped and doped monolayer and bilayer graphene: Selection rules and organizing principle among competing orders, *Phys. Rev. B* **103**, 205135 (2021).
- [12] M. O. Goerbig, J. N. Fuchs, G. Montambaux, and F. Piechon, Tilted anisotropic Dirac cones in quinoid-type graphene and  $\alpha - (\text{BEDT-TTF})_2\text{I}_3$ , *Phys. Rev. B* **78**, 045415 (2008).
- [13] M. O. Goerbig, Electronic properties of graphene in a strong magnetic field, *Rev. Mod. Phys.* **83**, 1193 (2011).
- [14] H. Caldas, J. L. Kneur, M. B. Pinto, and R. O. Ramos, Critical dopant concentration in polyacetylene and phase diagram from a continuous four-Fermi model, *Phys. Rev. B* **77**, 205109 (2008).
- [15] H. Caldas and R. O. Ramos, Magnetization of planar four-fermion systems, *Phys. Rev. B* **80**, 115428 (2009).
- [16] J. L. Kneur, M. B. Pinto, R. O. Ramos, and E. Staudt, Emergence of tricritical point and liquid gas phase in the massless 2+1 dimensional Gross-Neveu model, *Phys. Rev. D* **76**, 045020 (2007).
- [17] J. L. Kneur, M. B. Pinto, R. O. Ramos, and E. Staudt, Updating the phase diagram of the Gross-Neveu model in 2+1 dimensions, *Phys. Lett. B* **657**, 136 (2007).
- [18] J. L. Kneur, M. B. Pinto, and R. O. Ramos, Phase diagram of the magnetized planar Gross-Neveu model beyond the large- $N$  approximation, *Phys. Rev. D* **88**, 045005 (2013).
- [19] R. O. Ramos and P. H. A. Manso, Chiral phase transition in a planar four-fermion model in a tilted magnetic field, *Phys. Rev. D* **87**, 125014 (2013).
- [20] K. G. Klimenko, R. N. Zhokhov, and V. C. Zhukovsky, Superconducting phase transitions induced by chemical potential in (2+1)-dimensional four-fermion quantum field theory, *Phys. Rev. D* **86**, 105010 (2012).
- [21] K. G. Klimenko and R. N. Zhokhov, Magnetic catalysis effect in the (2+1)-dimensional Gross-Neveu model with Zeeman interaction, *Phys. Rev. D* **88**, 105015 (2013).
- [22] D. Ebert, K. G. Klimenko, P. B. Kolmakov, and V. C. Zhukovsky, Phase transitions in hexagonal, graphenelike lattice sheets and nanotubes under the influence of external conditions, *Ann. Phys.* **371**, 254 (2016).
- [23] D. Ebert, T. G. Khunjua, K. G. Klimenko, and V. C. Zhukovsky, Competition and duality correspondence between chiral and superconducting channels in (2+1)-dimensional four-fermion models with fermion number and chiral chemical potentials, *Phys. Rev. D* **93**, 105022 (2016).
- [24] V. C. Zhukovsky, K. G. Klimenko, and T. G. Khunjua, Superconductivity in chiral-asymmetric matter within the (2+1)-dimensional four-fermion model, *Moscow Univ. Phys. Bull.* **72**, 250 (2017).
- [25] N. Zerf, L. N. Mihaila, P. Marquard, I. F. Herbut, and M. M. Scherer, Four-loop critical exponents for the Gross-Neveu-Yukawa models, *Phys. Rev. D* **96**, 096010 (2017).
- [26] L. Fernández, V. Alves, M. Gomes, L. O. Nascimento, and F. Peña, Influence of the four-fermion interactions in a (2+1)-D massive electron system, *Phys. Rev. D* **103**, 105016 (2021).
- [27] J. E. Drut and D. T. Son, Renormalization group flow of quartic perturbations in graphene: Strong coupling and large- $N$  limits, *Phys. Rev. B* **77**, 075115 (2008).
- [28] V. Juričić, I. F. Herbut, and G. W. Semenoff, Coulomb interaction at the metal-insulator critical point in graphene, *Phys. Rev. B* **80**, 081405(R) (2009).
- [29] I. F. Herbut, V. Juričić, and O. Vafek, Relativistic Mott criticality in graphene, *Phys. Rev. B* **80**, 075432 (2009).
- [30] H. Rostami and V. Juričić, Probing quantum criticality using nonlinear Hall effect in a metallic Dirac system, *Phys. Rev. Res.* **2**, 013069 (2020).
- [31] T. G. Khunjua, K. G. Klimenko, and R. N. Zhokhov, Composite operator approach to dynamical mass generation in the (2 + 1)-dimensional Gross-Neveu model, *Intl. J. Mod. Phys. A* **36**, 2150231 (2021).
- [32] T. G. Khunjua, K. G. Klimenko, and R. N. Zhokhov, Spontaneous non-Hermiticity in the (2+1)-dimensional Gross-Neveu model, *Phys. Rev. D* **105**, 025014 (2022).
- [33] Y. Cao, V. Fatemi, S. Fang *et al.*, Unconventional superconductivity in magic-angle graphene superlattices, *Nature (London)* **556**, 43 (2018).
- [34] H. Zhou, T. Xie, T. Taniguchi *et al.*, Superconductivity in rhombohedral trilayer graphene, *Nature (London)* **598**, 434 (2021).
- [35] J. M. Park, Y. Cao, K. Watanabe *et al.*, Tunable strongly coupled superconductivity in magic-angle twisted trilayer graphene, *Nature (London)* **590**, 249 (2021).
- [36] Z. Hao *et al.*, Electric field-tunable superconductivity in alternating-twist magic-angle trilayer graphene, *Science* **371**, 1133 (2021).
- [37] Y. M. P. Gomes and R. O. Ramos, Tilted Dirac cone effects and chiral symmetry breaking in a planar four-fermion model, *Phys. Rev. B* **104**, 245111 (2021).
- [38] M. Hirata *et al.*, Observation of an anisotropic Dirac cone reshaping and ferrimagnetic spin polarization

- in an organic conductor, [Nat. Commun.](#) **7**, 12666 (2016).
- [39] M. Hirata, A. Kobayashi, C. Berthier, and K. Kanoda, Interacting chiral electrons at the 2D Dirac points: A review, [Rep. Prog. Phys.](#) **84**, 036502 (2021).
- [40] A. A. Burkov, Chiral anomaly and transport in Weyl metals, [J. Phys.: Condens. Matter](#) **27**, 113201 (2015).
- [41] M. Offidani and A. Ferreira, Anomalous Hall effect in 2D Dirac Materials, [Phys. Rev. Lett.](#) **121**, 126802 (2018).